

Influence of the reagents' ratio on photoelectric and optical properties of perovskite films for photovoltaics

V.P. Kostylyov^{1,*}, A.V. Sachenko¹, I.O. Sokolovskiy¹, V.M. Vlasiuk¹, P.V. Torchyniuk², O.I. V'yunov², A.G. Belous², A.I. Shkrebti³

¹V. Lashkaryov Institute of Semiconductor Physics, NAS of Ukraine, 41, prospect Nauky, 03680 Kyiv, Ukraine

²V. Vernadsky Institute of General and Inorganic Chemistry, NAS of Ukraine, 32/34, prospect Palladina, 03142 Kyiv, Ukraine

³Ontario Tech University, 2000 Simcoe St. N., Oshawa, ON, L1G 0C5, Canada

*Corresponding author e-mail: vkostylyov@ukr.net

Abstract. The properties of the synthesized films of organic-inorganic perovskites $\text{CH}_3\text{NH}_3\text{PbI}_3$ obtained at various ratios of starting reagents (PbI_2 and $\text{CH}_3\text{NH}_3\text{I}$) have been studied. As a solvent, we used chemically pure dried dimethylformamide (DMF). Organic-inorganic perovskites are promising for photovoltaic applications. It has been shown that regardless of the ratio of the starting reagents, single-phase perovskites are formed, at the same time the microstructure of the films changes significantly. It has been reported photoelectric and optical properties of synthesized films, namely: experimental and theoretical spectral dependences of the low-signal surface photovoltage and transmission. The band gap and the Urbach parameter dependence on the ratio of precursors were determined. It has been found that the materials' band gap depends on the ratio of precursors and equals to 1.59, 1.62 and 1.57 eV, while the characteristic Urbach energy equals to 18, 19 and 22 meV for the $\text{PbI}_2:\text{CH}_3\text{NH}_3\text{I}$ films with PbI_2 ratio of 1:1, 1:2 and 1:3, respectively. It has been ascertained that the spectral dependences of the low-signal surface photovoltage are much more sensitive to the material microstructure and its electronic structure close to the absorption edge, while the optical transmission spectra are not so sensitive. The limiting value of the short-circuit current density for the films with different PbI_2 and $\text{CH}_3\text{NH}_3\text{I}$ ratios has been determined.

Keywords: perovskites, surface photovoltage spectroscopy, optical properties.

<https://doi.org/10.15407/spqeo24.03.295>

PACS 73.61-r, 73.50.Pz, 72.40.+w, 73.43.Cd, 73.50.Gr, 42.25.Gy, 42.25.Bs, 81.07.Pr

Manuscript received 26.04.21; revised version received 25.06.21; accepted for publication 18.08.21; published online 26.08.21.

1. Introduction

In the future traditional approaches to energy generation that involve the burning of fossil fuels (oil, gas, coal) will not be able to meet the energy needs. Moreover, the use of such energy sources leads to significant pollution of the environment, and it can put humanity on the brink of survival. The use of photovoltaic solar cells (PV SC) to generate electricity is promising. Currently, to produce solar cells, silicon-based elements [1, 2] and elements based on compounds A^3B^5 (GaAs, InP) are used [3].

One of the promising candidates for manufacturing the solar cells are organic-inorganic perovskites ABX_3 , where A is mainly methyl ammonium (CH_3NH_3), B is Pb, Sn, and X is F, Cl, Br, I. These materials are characterized by direct interband optical transitions, so they have a high absorption coefficient, and PV SC based on perovskite belong to the second generation of thin-

film solar cells [4]. An important advantage of such elements is simpler and cheaper technology for manufacturing the solar cells based on organic-inorganic perovskites, as compared to silicon-based elements. Over the recent 10 years, the power conversion efficiency (PCE) of solar cells based on perovskites has increased from 3% to 25.2% (and to 28% in tandem architecture) [5, 6]. However, today the stability of these elements under the action of moisture, heat, and radiation is low, which creates significant obstacles to their implementation in practice.

The films of organic-inorganic perovskites can be used in the development of various optical systems, as well as in the elements of solar energy conversion. Therefore, preparation of dense single-phase films is very important. In this case, the perovskite thin films can be fabricated by variety of different deposition methods: spin-coating, application by immersion in solution, film

casting, spraying, or vacuum deposition, one-stage deposition [7], two-stage sequential deposition [8], the method of Lewis basic adducts for lead (II) iodide [9], treatment of vapor-containing solutions [10], electrospray deposition [11], *etc.*

Typically, the starting reagents (PbI_2 , $\text{CH}_3\text{NH}_3\text{I}$) are dissolved in organic solvents, *e.g.*, N,N-dimethylformamide (DMF), γ -butyrolactone (GBL), dimethyl sulfoxide (DMSO). To deposit perovskite films, the resulting solution is deposited onto a heated substrate. All the above factors, namely, the application methods and solvents impact the crystallization process significantly, resulting in the films with different morphology (grain shape and size), and, different crystal structural defects, both at the grain boundaries and inside the films [12]. In polycrystalline films, grain size and orientation, as well as defect types effect significantly the films' optical and photoelectric characteristics, being most crucial for photoconversion. As a rule, the optical and photoelectric characteristics are studied using already fabricated SCs, consisting of several layers in addition to the perovskite film (used as an absorber layer). As a result, the commonly measured characteristics are integrated, and it is often difficult to separate contributions of individual layers. Understanding the individual layer contribution, however, is important when SC fabrication technologies are being developed.

The role of selective contacts to $\text{CH}_3\text{NH}_3\text{PbI}_{3-x}\text{Cl}_x$ was studied in [13] using surface photovoltage (SPV) spectroscopy. The photovoltage at the operation surface V_{ph} was measured using the contactless way in the large signal mode (the SPV signal varied within tens to hundreds mV, *i.e.*, $V_{ph} \gg kT/q$). In [14, 15], the Goodman approach was used to determine the diffusion length of the minority carriers in perovskite films from the spectral dependences of the surface photovoltage $V_{ph}(\lambda)$. Low-signal SPV spectroscopy ($V_{ph}(\lambda) \ll kT/q$) together with transmission and reflection measurements was used to determine the band gap and the characteristic Urbach energy [16]. It was shown that the spectral dependence of the low-signal surface photovoltage is proportional to the external quantum efficiency $EQE(\lambda)$, and the minority carriers diffusion length exceeds the thickness of the perovskite film (400 nm). The results of [13–16] illustrate the informativeness of SPV spectroscopy to study and characterize perovskites films and perovskite based SCs.

The goal of this work is to study properties of perovskite $\text{CH}_3\text{NH}_3\text{PbI}_{2.98}\text{Cl}_{0.02}$ films for several PbI_2 and $\text{CH}_3\text{NH}_3\text{I}$ precursors' ratios in the process of the films synthesis from DMF solvent. We prepared perovskite $\text{CH}_3\text{NH}_3\text{PbI}_{2.98}\text{Cl}_{0.02}$ films and investigated their spectral dependences of the optical transmission and the low-signal surface photovoltage for the precursors' ratios of 1:1, 1:2 and 1:3. It was found that the spectral dependences of the low-signal surface photovoltage are sensitive to the material microstructure. The band gap and characteristic Urbach energy for all the precursor ratios are determined. It is shown that the minority carriers diffusion length exceeds the perovskite film thickness for all the samples considered.

2. Research methodology

2.1. Methods of synthesis

Lead iodide PbI_2 , methylammonium chloride $\text{CH}_3\text{NH}_3\text{Cl}$ (chemically pure, CP) and pre-synthesized methylammonium iodide $\text{CH}_3\text{NH}_3\text{I}$ were used as starting reagents for the synthesis [17]. To stabilize the perovskite structure, iodine was partially substituted with chlorine [18]. As a solvent, we used chemically pure dried dimethylformamide (DMF). To obtain $\text{CH}_3\text{NH}_3\text{PbI}_{2.98}\text{Cl}_{0.02}$ films, the starting reagents PbI_2 , $\text{CH}_3\text{NH}_3\text{I}$ and $\text{CH}_3\text{NH}_3\text{Cl}$ in ratios of 1:0.98:0.02 (hereinafter 1:1); 1:1.98:0.02 (1:2); 1:2.98:0.02 (1:3) were dissolved in DMF and stirred at 70 °C for 1 hour. The synthesis was performed in a dry box. The resulting transparent solution was deposited onto pre-cleaned substrates of glass and glass with ITO coating (the latter is hereinafter referred to as ITO/glass) by spin-coating at the speed 1200 rpm for 30 s. Heat treatment of the films was performed on a pre-heated hot plate within the temperature range 90 °C up to 190 °C for 15 min.

2.2. Measuring methods

The obtained films were characterized using X-ray diffraction. X-ray patterns of the powders were measured using DRON-4-07 spectrometer (CuK α radiation, 30 kV, 30 mA) within the range $2\Theta = 5^\circ \dots 70^\circ$ with the step 0.05° and 3 s exposure time. The unit cell parameters were determined from the X-ray data by Rietveld refinements method by using a full profile fitting procedure. The microstructure of the synthesized films was studied by scanning electron microscopy using SEC mini-SEM SNE 4500MB.

The thickness of the films was determined using a microinterferometer MII4.

Spectral dependences of the low-signal surface photovoltage $V_{ph}(\lambda)$ ($V_{ph} \ll kT/q = 0.025$ V) were measured within the wavelength range $\Delta\lambda = 400 \dots 900$ nm on the samples of $\text{CH}_3\text{NH}_3\text{PbI}_{2.98}\text{Cl}_{0.02}$ perovskite films, fabricated on the glass substrate with ITO sublayer. The spectra were measured at a constant photon flux of the monochromatic light, modulated by the frequency of 20 Hz. An alternating voltage with a frequency of 20 Hz was used as a reference signal to control an oscillating beam splitter. The spectra proportional to the values of external and internal quantum efficiency were obtained. Surface photovoltage measurements were performed non-destructively by using a clamping capacitive electrode made of mica $\sim 5\text{-}\mu\text{m}$ thick with a deposited semitransparent ITO layer of the area close to $\sim 7 \times 7$ mm, as described in [16]. To improve the signal-to-noise ratio, amplification on a variable signal with subsequent synchronous detection (lock-in amplifier) was used. The amplitude of the periodic modulated alternating signal $V_{ph}(\lambda)$ did not exceed 20 μV in any case.

The reflection coefficient from the surface of the perovskite film at the wavelength 632.8 nm was estimated. Measurements indicate the diffuse character of reflection with quite a small light reflection coefficient, its estimated value was $\sim 8\%$.

The transmission spectra were measured within the wavelength range $\Delta\lambda = 400\text{...}900$ nm by using the perovskite film samples $\text{CH}_3\text{NH}_3\text{PbI}_{2.98}\text{Cl}_{0.02}$ deposited onto glass without the ITO sublayer. A silicon photodiode was used as a reference photodetector. In general, when measuring the transmittance of objects with a profiled (textured) surface, it is necessary to use integrating sphere. In our measurements, the integrating sphere was not used. The reasons for this were as follows: (1) the light beam exited out from the side of substrate, where the surface profile of the perovskite film was closer to flat, since it was imposed on the polished substrate and scattered much less; (2) the sample was mounted onto the frame of the reference photodetector, and the distance between the reference photodetector which measures the intensity of the transmitted beam and the sample did not exceed 1 mm. The active area of the photodetector was 5×5 mm, which is less than the area of the perovskite film. Thus, almost complete capture (no less than 86%) of the transmitted radiation was ensured.

Since the transmittance measurements were used to additionally verify the main data obtained using surface photovoltage spectroscopy, these transmittance measurements provided acceptable accuracy.

The spectral measurements were performed using the equipment for determining the spectral characteristics of photoconverters at the Testing Center for Photoconverters and Photovoltaic Batteries of the V. Lashkaryov Institute of Semiconductor Physics, National Academy of Sciences of Ukraine. The testing equipment has been certified by the authorized bodies of State Committee of Ukraine for Technical Regulation and Consumer Policy (Derzhspozhyvstandart).

3. Results and discussion

Typically, perovskite $\text{CH}_3\text{NH}_3\text{PbI}_3$ is obtained at a ratio of PbI_2 and $\text{CH}_3\text{NH}_3\text{I}$ – 1:1. In this work, $\text{CH}_3\text{NH}_3\text{PbI}_{2.98}\text{Cl}_{0.02}$ perovskite films were synthesized for the precursor ratios of 1:1, 1:2 and 1:3. After the synthesis, the films' microstructural, optical and photoelectric characteristics were investigated. The unit cell parameters of the $\text{CH}_3\text{NH}_3\text{PbI}_{2.98}\text{Cl}_{0.02}$ materials have

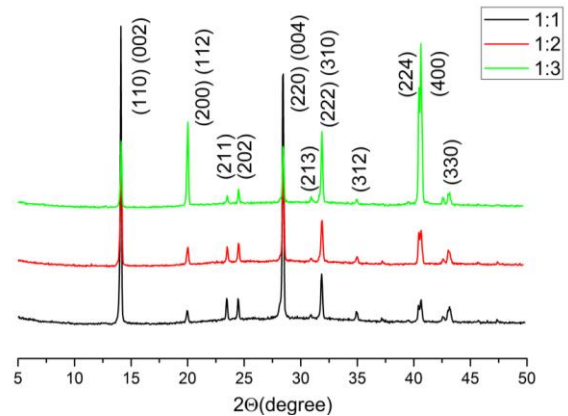


Fig. 1. Experimental X-ray diffractograms of $\text{CH}_3\text{NH}_3\text{PbI}_{2.98}\text{Cl}_{0.02}$ film samples prepared using different ratios of initial reagents. Miller indices are given in the brackets.

been determined by the full-profile Rietveld method by using X-ray diffraction patterns of the single-phase samples (Fig. 1).

Calculations of the structural parameters indicate that this diffractogram corresponds to the tetragonal symmetry (space group $I4/mcm$, 140), which agrees with the literature [19]. The unit cell parameters of the films of organic-inorganic perovskites are shown in Table 1. The results of Energy-Dispersive X-ray (EDX) spectroscopic measurements showed that the intensity ratio of the Pb and I peaks is the same for samples, synthesized with different precursor ratios. That is, the elemental composition of the perovskite film is stoichiometric, regardless of $\text{CH}_3\text{NH}_3\text{I}$ excess [18].

Fig. 2 shows that the microstructure of the synthesized films significantly depends on the precursors' ratio. In particular, for the precursors' ratio 1:1 the films consist of needles, parallel to the substrate (Fig. 2a). At the 1:2 ratio the films contain particles in the form of a maple leaf (Fig. 2b), and rounded particles are formed at the 1:3 precursors' ratio (Fig. 2c).

The obtained films had porosity, but the porosity value was not determined numerically in the work. The porosity of perovskite films can be controlled by changing the ratio of starting reagents PbI_2 and $\text{CH}_3\text{NH}_3\text{I}$.

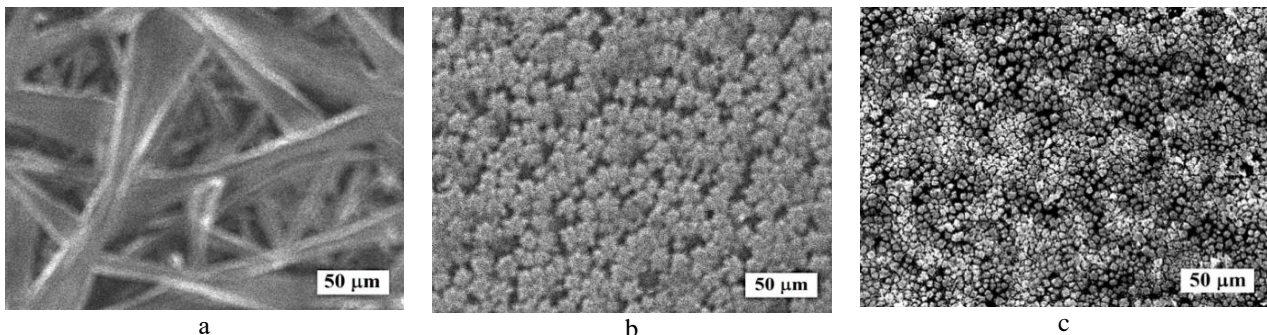


Fig. 2. The microstructure of $\text{CH}_3\text{NH}_3\text{PbI}_{2.98}\text{Cl}_{0.02}$ films prepared with different ratios of PbI_2 and $\text{CH}_3\text{NH}_3\text{I}$ and subsequent heat treatment at (a) 1:1 – 115 °C, (b) 1:2 – 170 °C and (c) 1:3 – 175 °C.

Table 1. The structural parameters of the organic-inorganic perovskites $\text{CH}_3\text{NH}_3\text{PbI}_{2.98}\text{Cl}_{0.02}$ at different ratios of starting reagents PbI_2 and $\text{CH}_3\text{NH}_3\text{I}$ (1:1, 1:2, 1:3) prepared in DMF as a solvent.

Ratios of starting reagents	1:1	1:2	1:3
Unit cell parameters			
$a, \text{Å}$	8.8657(9)	8.878(1)	8.884(1)
$c, \text{Å}$	12.653(2)	12.669(6)	12.638(4)
$V, \text{Å}^3$	994.5(3)	998.6(5)	997.5(4)
Single-phase region	115–120 °C	170–175 °C	175–180 °C
Deposition temperature	115 °C	170 °C	175 °C

In the central part of the sample, the film had a uniform thickness of about 400 nm. The thickness of the edges varied significantly, which is typical when using the centrifugation method.

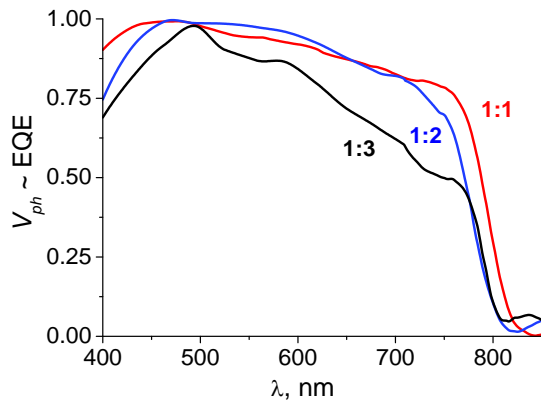
We found that the amplitude of the low-signal surface photovoltage $V_{ph}(\lambda)$ of the samples under study decreases with an increase of the $\text{CH}_3\text{NH}_3\text{I}$ fraction from 1 to 3 during the synthesis of the perovskite film. The $V_{ph}(\lambda)$ values are 8.1 μV at (1:1), 0.96 μV at (1:2), and 0.41 μV at (1:3). This indicates a decrease in the surface charge and the surface band bending with an increase in the $\text{CH}_3\text{NH}_3\text{I}$ fraction.

The experimental spectral dependences of the low-signal surface photovoltage $V_{ph}(\lambda)$ (normalized to photon flux and to unity at the maximum) are shown in Fig. 3 for the PbI_2 to $\text{CH}_3\text{NH}_3\text{I}$ ratios of 1:1, 1:2 and 1:3.

As shown in [16], the spectral dependences of the low-signal surface photovoltage, measured at a constant photon flux of the monochromatic light, are proportional to the spectral dependences of the external quantum efficiency $V_{ph}(\lambda) \sim EQE(\lambda)$, that is we can write:

$$V_{ph}(\lambda) = A(\varphi_s, \lambda)EQE(\lambda), \quad (1)$$

where $A(\varphi_s, \lambda)$ is the coefficient of proportionality, which depends on the sign and the value of the band bending φ_s on the illuminated surface of the film.


Fig. 3. Experimental spectra of the low-signal surface photovoltage $V_{ph}(\lambda)$ normalized to photon flux and to unity at the maximum.

Additionally, the perovskite films surface is naturally textured (see Fig. 2). As a result, the experimental (normalized to unity) dependences $V_{ph}(\lambda)$ at the absorption edge can be described by the empirical formula:

$$V_{ph}(\lambda) = EQE(\lambda) = \left[1 + b/4\alpha(\lambda) \cdot d \cdot (n_r(\lambda))^2\right]^{-1}, \quad (2)$$

where $\alpha(\lambda)$ is the light absorption coefficient, d – film thickness, $n_r(\lambda)$ – its refractive index, and b – dimensionless coefficient, larger than 1. The parameter b corresponds to the ratio of the probability of photon, exiting from a sample under consideration, to the corresponding probability of its exit in the case of a perfectly randomized surface, considered in [20, 21]. We emphasize that for the expression (2) to be accurate, it is necessary that the diffusion length of the minority carriers L significantly exceeds the film thickness d .

In the limiting case of $b = 1$, the expression (2) under the assumption that one photon generates one electron-hole pair is equivalent to the well-known Yablonoitch formula for absorption [22]:

$$A(\lambda) = \frac{\alpha(\lambda)}{\alpha(\lambda) + 1/4n_r^2d} = \left[1 + 1/4\alpha(\lambda)n_r^2d\right]^{-1}. \quad (3)$$

Fig. 3 demonstrates that the low-signal surface photovoltage spectra significantly depend on the PbI_2 and $\text{CH}_3\text{NH}_3\text{I}$ precursors' ratio, most noticeably in the long-wave region of the $V_{ph}(\lambda)$ spectral curves. The difference becomes even stronger close to the absorption edge, which is defined by the band gap value. In addition, it was previously found that the Urbach effect occurs for the perovskite films at the edge of absorption. This effect characterizes the films' structural imperfection. The empirical dependence of the absorption coefficient on the photon energy in this region has the form:

$$\alpha_{Ur} = \alpha_{Ur0} \exp(E_{ph}/E_0), \quad (4)$$

where α_{Ur0} is the initial absorption coefficient, E_{ph} – photon energy, E_0 – characteristic energy, which is tens of meV for a small deviation from the perfect films. Therefore, to describe theoretically the long-wave part of the spectrum $V_{ph}(\lambda)$, we took into account these mechanisms.

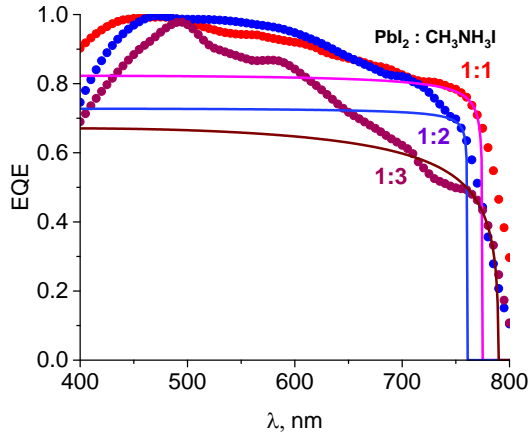


Fig. 4. Experimental (points) and theoretical (lines) spectra of the normalized low-signal surface photovoltage.

Since perovskites are direct-band gap semiconductors, according to [23] at the edge of absorption, the absorption coefficient is determined using the formula

$$\alpha(\lambda) = B \frac{(1239.7/\lambda - E_g)^{1/2}}{1239.7/\lambda}, \quad (5)$$

where B is a constant, E_g – band gap, and λ – wavelength in nanometers. The exponent power $1/2$ in the numerator, depending on the dominant optical transitions, in the general case can take values from $1/2$ up to $3/2$.

Fig. 4 shows experimental spectra of the low-signal surface photovoltage $V_{ph}(\lambda)$ (normalized to the photon flux and to unity) and the theoretical plots, calculated using Eq. (5). Theoretical spectra are aligned to the experimental ones in the vicinity of the absorption edge. From the fitting, we can determine the films' band gap for the direct optical transitions, and how the gap depends on the film synthesis conditions. In particular, the band gap is 1.59, 1.62 and 1.57 eV for the PbI_2 to CH_3NH_3I ratios of 1:1, 1:2 and 1:3, respectively. Also, it can be seen that the theoretical dependences for the longer wavelengths are steeper, while the experimental ones are extended in the long-wave region of the spectrum. This shift is explained by the Urbach effect, confirmed by the data shown in Fig. 5, where the long-wave part of the spectrum $V_{ph}(\lambda)$ is plotted ($\log(V_{ph})$ vs. photon energy E). It can be seen that according to (4) $\log(V_{ph})$ is linear with E in the absorption edge vicinity. This allows to determine the characteristic parameters E_0 and α_{Urb} for the synthesized films, depending on the CH_3NH_3I excess, the parameters are shown in Table 2 below.

Table 2. Characteristic parameters of the Urbach effect.

$PbI_2:CH_3NH_3I$	E_0 , meV	$\alpha_{Urb} \cdot 10^4$, cm^{-1}
1:1	18	4.5
1:2	19	1.6
1:3	22	3.6

From the Urbach characteristic energy, one can conclude that a disorder of the synthesized films is moderate, and the disorder increases with increase of CH_3NH_3I excess in the initial reagents.

Typically, the dependence of the inverse value of the low-signal surface photovoltage V_{ph}^{-1} , normalized to the photons flux, on the inverse absorption coefficient α^{-1} is used to determine the diffusion length of minority carriers [24]. This is usually made by determining the cut-off on the abscissa axis α^{-1} of the linear dependence region V_{ph}^{-1} near the absorption edge. It was shown in [16] that for profiled (textured) surfaces, the diffusion length L can be approximately estimated when the sample thickness significantly exceeds L : $d \geq (3...4)L$. In the case of large values of L compared to the sample thickness, the expression (2) should be used. In this case, the cut-off value equals

$$L_{ph} = 4n_r^2 d / b \quad (6)$$

and determines the mean path length L_{ph} of the long-wave photon before its photoactive absorption. Then, if the cut-off exceeds the sample thickness, this indicates a longer diffusion length of the minority carriers compared to the sample thickness. When this length exceeds significantly the sample thickness, we have to use the expression (2) for the textured surface, or expression

$$IQE_{nt}(\lambda) = 1 - \exp(-2\alpha(\lambda)d) \quad (7)$$

for the mirror surface with 100% reflection from the back surface.

Very informative experimental dependence of the inverse photovoltage V_{ph}^{-1} on the inverse absorption coefficient α^{-1} for films with different ratio of precursors

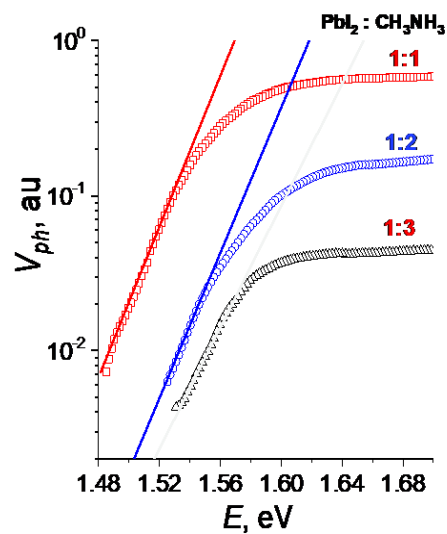


Fig. 5. Urbach effect parameters determination from experimental surface photovoltage $V_{ph}(E)$ spectra for the synthesized $CH_3NH_3PbI_{0.98}Cl_{0.02}$ films (points). Lines: theory, calculated using Eq. (4).

is demonstrated in next Fig. 6. To draw Fig. 6, we used the dependence $\alpha(\lambda)$, as measured in [25], with a correction (which was defined by us) for the value of the band gap, by parallel shifting along the horizontal coordinate axis, and including the Urbach effect, using Eq. (4) with the parameters from Table 2. The following cut-off values obtained for different precursor ratios are: $4.42 \mu\text{m}$ (1:1), $1.19 \mu\text{m}$ (1:2) and $4.75 \mu\text{m}$ (1:3). The obtained cut-off values indicate a significant excess – 12 (1:3), 11 (1:1) and 3 (1:2) times greater than the sample thickness – 400 nm ($0.4 \mu\text{m}$). This allowed us to conclude that the diffusion length of minority carriers in the samples under study significantly exceeds the sample thickness, and, taking into account the presence of a naturally profiled surface, the empirical formula (2) should be used to describe their long-wave edge. The largest, practically close cut-off values are observed at the ratio of the initial reagents (1:1) and (1:3), which indicates their noticeably higher quality and longer diffusion length of minority carriers, as compared with the ratio (1:2).

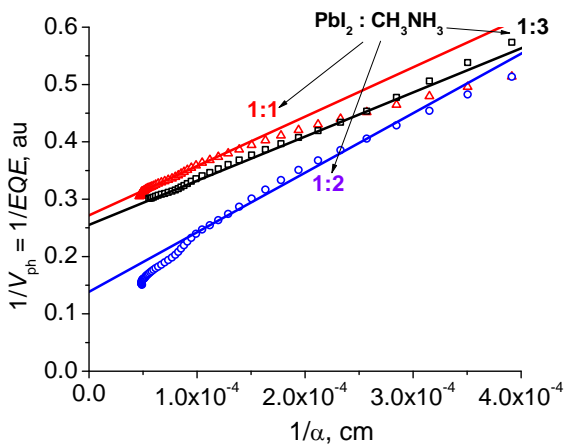


Fig. 6. Experimental dependences of V_{ph}^{-1} on α^{-1} for films with different ratio of precursors.

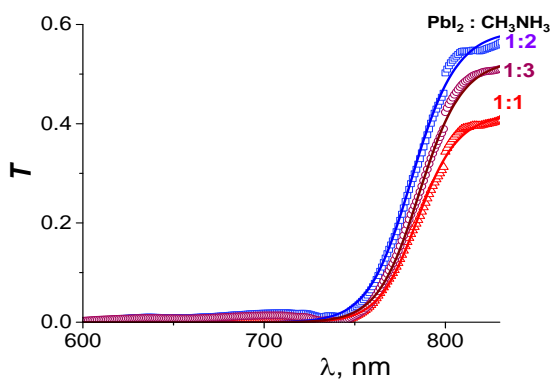


Fig. 7. Experimental (symbols) and theoretical (lines) spectral dependences of the samples' transmission for different ratios of precursors.

Using the expression (6), one can find the value of the parameter b , which is equal to 2.36 (1:1), 8.76 (1:2) and 2.17 (1:3). The obtained values of the parameters indicate a high efficiency capture of light in the case of the ratio of reagents (1:1) and (1:3) and significantly worse – for the ratio (1:2).

Fig. 7 demonstrates experimental spectral dependences of the transmission coefficients of the perovskite films for the precursors' ratios of 1:1, 1:2 and 1:3 in the λ range of 600 to 830 nm. It is seen from the figure that increase of the transmission coefficient of the film with the ratio of 1:1 has the largest shift, and the smallest shift is inherent to the film with the ratio 1:2.

The porosity of the perovskite layer leads to an increase in transmission, which is especially noticeable within the spectral region of strong absorption (wavelength range 400...750 nm). It was manifested in our case in the form of appearance of a “background”, especially in the presence of through pores. This effect requires further investigation and can possibly be used to determine the porosity of the layers.

Fig. 7 also shows the theoretical dependences of the films transmittance for perovskites with PbI_2 and $\text{CH}_3\text{NH}_3\text{I}$ ratios 1:1, 1:2 and 1:3. The calculation was performed using the approximate formula:

$$T(\lambda) \approx 1 - R(\lambda) - EQE(\lambda), \quad (8)$$

where $R(\lambda)$ is the reflection coefficient from the perovskite film. The spectral dependence $R(\lambda)$ was obtained by calculation taking into account multiple reflections from the front and back surfaces [26]:

$$R(\lambda) = r(\lambda) + r(\lambda)T(\lambda)\exp(-\alpha(\lambda)d), \quad (9)$$

where $r(\lambda)$ is the reflection coefficient from the front surface of perovskite film.

The reflection coefficient from the front surface $r(\lambda)$ was calculated using the Fresnel formulas with the literature data for the complex refractive index [27].

The formula (8) is obtained from (10)

$$T(\lambda) = 1 - R(\lambda) - A(\lambda) \leq 1 - R(\lambda) - EQE(\lambda), \quad (10)$$

Since absorption $A(\lambda)$ is in proportion to the amount of all photogenerated carriers, which is equal to the amount of absorbed photons, and $EQE(\lambda)$ is proportional to all photogenerated carriers minus the recombined ones. In the case of long diffusion lengths of minority carriers, recombination is low and is taken into account by the coefficient b in the equation (2).

As can be seen from Fig. 7, in the vicinity of wavelengths 740 to 820 nm, a good agreement of the experiment and calculation is achieved for perovskites with all PbI_2 to $\text{CH}_3\text{NH}_3\text{I}$ ratios considered, namely, 1:1, 1:2 and 1:3. It should be noted that the transmission data are also consistent with the corresponding data from the spectra of low-signal surface photovoltage.

Note that the short-circuit current density J_{SC} for AM1.5 conditions can be determined from the following expression [28]:

$$J_{SC} = q \int_{\lambda_0}^{\lambda_m} I_{AM1.5}(\lambda) EQE(\lambda) d\lambda, \quad (11)$$

where λ_0 is the short-wave absorption edge, λ_m – long-wave absorption edge, $EQE(\lambda)$ – external quantum efficiency, $I_{AM1.5}(\lambda)$ – spectral density of the photon flux under AM1.5.

Assume that the experimental photovoltages $V_{ph}(\lambda)$, normalized to the photon flux and to the maximum value, are the limiting values for $EQE(\lambda)$ in the case of different perovskite films. Then, using the formula (11), we can calculate the J_{SC} limiting value for the films with different ratios of initial reagents PbI_2 to CH_3NH_3I . We obtained accordingly: $J_{SC1} = 26.1 \text{ mA/cm}^2$ (1:1), $J_{SC2} = 24.9 \text{ mA/cm}^2$ (1:2) and $J_{SC3} = 21.8 \text{ mA/cm}^2$ (1:3). Thus, the highest limiting value of short-circuit current can be obtained with a 1:1 ratio between PbI_2 to CH_3NH_3I .

4. Conclusions

We have investigated photoelectric and optical properties of perovskite $CH_3NH_3PbI_{2.98}Cl_{0.02}$ films depending on the ratio of the precursors PbI_2 and CH_3NH_3I during their synthesis.

It has been found that the microstructure of perovskite films significantly depends on the ratio of $PbI_2:CH_3NH_3I$, despite the fact that the elemental composition of the perovskite film remains stoichiometric. When the ratio of precursors is 1:1, the structure is needle-shaped. At the ratio 1:2, the films consist of faceted crystallites in the amorphous matrix, and at the ratio 1:3 contain smaller crystallites. This microstructure of perovskite films leads to the appearance of surface microrelief, and, accordingly, to improved light capture in the long-wave range. The best capture is achieved in films with the ratio of precursors 1:1, and the worst – in the case of 1:2.

It has been ascertained that the band gap of the perovskite films depends on the ratio of precursors and equals to 1.59, 1.62 and 1.57 eV for films with PbI_2 to CH_3NH_3I ratios of 1:1, 1:2 and 1:3, respectively.

Measurement of the Urbach characteristic energy showed that the structural disorder in the synthesized films is moderate, and this disorder enhances with increasing the excess of CH_3NH_3I in the initial reagents.

We have found that the amplitude of the low-signal surface photovoltage $V_{ph}(\lambda)$ decreases with increasing the proportion of CH_3NH_3I from 1 to 3 during the synthesis of the perovskite film. The $V_{ph}(\lambda)$ amplitude values are $8.1 \mu\text{V}$ at (1:1), $0.96 \mu\text{V}$ at (1:2) and $0.41 \mu\text{V}$ at (1:3), which indicates a decrease of the surface charge and the initial surface band bending.

Also, it has been ascertained that the spectral dependences of the low-signal surface photovoltage $V_{ph}(\lambda)$ are much more sensitive to the microstructure and electronic structure within the region of absorption edge, as compared with the optical transmission spectra.

It has been shown that all the investigated films have longer diffusion length of the minority charge carriers as compared to the film thickness and are promising for applications in photovoltaics and optoelectronics.

References

1. Wang Z., Zhu X., Zuo S. *et al.* 27%-efficiency four-terminal perovskite/silicon tandem solar cells by sandwiched gold nanomesh. *Adv. Funct. Mater.* 2019. **30**. P. 1908298 (1–8). <https://doi.org/10.1002/adfm.201908298>.
2. Green M.A. Commercial progress and challenges for photovoltaics. *Nature Energy*. 2016. **1**, No 1. P. 1–4. <https://doi.org/10.1038/nenergy.2015.15>.
3. Green M.A., Dunlop E.D., Hohl-Ebinger J. *et al.* Solar cell efficiency tables (version 55). *Prog. Photovolt. Res. Appl.* 2020. **28**. P. 3–15. <https://doi.org/10.1002/ppa.3228>.
4. Green M.A. *Third Generation Photovoltaics: Advanced Solar Energy Conversion*. Springer, 2003.
5. Kojima A., Teshima K., Shirai Y. *et al.* Organometal halide perovskites as visible-light sensitizers for photovoltaic cells. *J. Am. Chem. Soc.* 2009. **131**. P. 6050–6051.
6. *Best Research-Cell Efficiency Chart*, URL: <https://www.nrel.gov/pv/cell-efficiency.html> (accessed 15 May, 2020).
7. Zhao Y., Zhu K. Charge transport and recombination in perovskite (CH_3NH_3) PbI_3 sensitized TiO_2 solar cells. *J. Phys. Chem. Lett.* 2013. **4**. P. 2880–2884. <https://doi.org/10.1021/jz401527q>.
8. Burschka J., Pellet N., Moon S.-J. *et al.* Sequential deposition as a route to high-performance perovskite-sensitized solar cells. *Nature*. 2013. **499**(7458). P. 316–319. <https://doi.org/10.1038/nature12340>.
9. Park N. Highly reproducible perovskite solar cells with average efficiency of 18.3% and best efficiency of 19.7% fabricated *via* lewis base adduct of lead(II) iodide. *J. Am. Chem. Soc.* 2015. **137**, No 27. P. 8696–8699. <https://doi.org/10.1021/jacs.5b04930>.
10. Liu M., Johnston M.B., Snaith H.J. Efficient planar heterojunction perovskite solar cells by vapour deposition. *Nature*. 2013. **501**(7467). P. 395–398. <https://doi.org/10.1038/nature12509>.
11. Kavadiya S., Niedzwiedzki D.M., Huang S. *et al.* Electro-spray-assisted fabrication of moisture-resistant and highly stable perovskite solar cells at ambient conditions. *Adv. Energy Mater.* 2017. **7**, No 18. P. 1700210 (1–9).
12. Belous A., Kobylanska S., V'yunov O. *et al.* Effect of non-stoichiometry of initial reagents on morphological and structural properties of perovskites $CH_3NH_3PbI_3$. *Nanoscale Res. Lett.* 2019. **14**, No 1. P. 4. <https://doi.org/10.1186/s11671-018-2841-6>.
13. Barnea L., Kirmayer S., Edri E., Hodes G., and Cahen D. Surface photovoltage spectroscopy study of organo-lead perovskite solar cells. *J. Phys. Chem. Lett.* 2014. **5**, No 14. P. 2408–2413. <https://doi.org/10.1021/jz501163r>.

14. Dittrich Th., Lang F., Shargaieva O. *et al.* Diffusion length of photo-generated charge carriers in layers and powders of $\text{CH}_3\text{NH}_3\text{PbI}_3$ perovskite. *Appl. Phys. Lett.* 2016. **109**. P. 073901 (1–4). <https://doi.org/10.1063/1.4960641>.
15. Wang J., Motaharifar E., Higgins M. *et al.* Revealing lattice and photocarrier dynamics of high-quality MAPbBr_3 single crystals by far infrared reflection and surface photovoltage spectroscopy. *J. Appl. Phys.* 2019. **125**. P. 025706 (1–7). <https://doi.org/10.1063/1.5072794>.
16. Kostylyov V.P., Sachenko A.V., Vlasiuk V.M. *et al.* Synthesis and investigation of the properties of organic-inorganic perovskite films with non-contact methods. *Ukr. J. Phys.* 2021. **66**, No. 5. P. 429–438. <https://doi.org/10.15407/ujpe66.5.429>.
17. Qiu J., Qiu Y., Yan K. *et al.* All-solid-state hybrid solar cells based on a new organometal halide perovskite sensitizer and one-dimensional TiO_2 nanowire arrays. *Nanoscale*. 2013. **5**, No 8. P. 3245–3248. <https://doi.org/10.1039/c3nr00218g>.
18. Belous A.G., V'yunov O.I., Kobylanskaya S.D., Ishchenko A.A., and Kulinich A.V. Influence of synthesis conditions on the morphology and spectral-luminescent properties of films of organic-inorganic perovskite $\text{CH}_3\text{NH}_3\text{PbI}_{2.98}\text{Cl}_{0.02}$. *Rus. J. Gen. Chem.* 2018. **88**, No 1. P. 114–119. <https://doi.org/10.1134/S1070363218010188>.
19. Kawamura Y., Mashiyama H., and Hasebe K. Structural study on cubic-tetragonal transition of $\text{CH}_3\text{NH}_3\text{PbI}_3$. *J. Phys. Soc. Jpn.* 2002. **71**, No 7. P. 1694–1697. <https://doi.org/10.1143/JPSJ.71.1694>.
20. Green M.A. Lambertian light trapping in textured solar cells and light-emitting diodes: analytical solutions. *Prog. Photovolt: Res. Appl.* 2002. **10**. P. 235–241. <https://doi.org/10.1002/pip.404>.
21. Tiedje T., Yablonoitch E., Cody G.D., and Brooks B.J. Limiting efficiency of silicon solar cells. *IEEE Trans. on Electron Devices*. 1984. **31**, No 5. P. 711–716. <https://doi.org/10.1109/T-ED.1984.21594>.
22. Yablonoitch E. Statistical ray optics. *J. Opt. Soc. Amer.* 1982. **72**, No 7. P. 899–907. <https://doi.org/10.1364/JOSA.72.000899>.
23. Mott N.F., Davis E.A. *Electronic Processes in Non Crystalline Materials*. Oxford Univ. Press, 1979.
24. ASTM Standard F391-90a, “Standard Test Method for Minority-Carrier Diffusion Length in Silicon by Measurement of Steady-State Surface Photovoltage,” *1996 Annual Book of ASTM Standards*, Am. Soc. Test. Mat., West Conshohocken, PA, 1996.
25. De Wolf S., Holovsky J., Moon So-Jin *et al.* Organometallic halide perovskites: Sharp optical absorption edge and its relation to photovoltaic performance. *J. Phys. Chem. Lett.* 2014. **5**, No 6. P. 1035–1039. <https://doi.org/10.1021/jz500279b>.
26. Schroder D.K. *Semiconductor Material and Device Characterization*. Wiley-IEEE Press, 2006.
27. Leguy A.M.A., Hu Y., Campoy-Quiles M. *et al.* Reversible hydration of $\text{CH}_3\text{NH}_3\text{PbI}_3$ in films, single crystals, and solar cells. *Chem. Matter*. 2015. **27**, No 9. No 3397–3407. <https://doi.org/10.1021/acs.chemmater.5b00660>.
28. Sachenko A.V., Kostylyov V.P., Vlasyuk V.M. *et al.* Peculiarities of photoconversion efficiency modeling in perovskite solar cells. *Techn. Phys. Lett.* 2017. **43**, No 7. P. 678–680. <https://doi.org/10.1134/S1063785017070240>.

Authors and CV



Kostylyov V.P. Professor, Doctor of Sciences (Phys & Math), Head of the Laboratory of Physical and Technical Fundamentals of Semiconductor Photovoltaics at the V. Lashkaryov Institute of Semiconductor Physics. He is the author of more than 250 scientific publications. The area of his scientific interests includes photovoltaics and betavoltaics, research, analysis and modelling of solar cells, testing the solar cells, characterization and metrology as well as characterization of the optical and recombination properties of photovoltaics materials. <https://orcid.org/0000-0002-1800-9471>



Sachenko A.V. Professor, Doctor of Sciences (Phys & Math), Chief Researcher of the Laboratory of Physical and Technical Fundamentals of Semiconductor Photovoltaics at the V. Lashkaryov Institute of Semiconductor Physics. He is the author of more than 300 scientific publications. His main research interests include

analysis, characterization, and modeling of silicon solar cells. <https://orcid.org/0000-0003-0170-7625>; avsachenko@gmail.com



Sokolovskiy I.O. PhD, Senior Researcher of the Laboratory of Physical and Technical Fundamentals of Semiconductor Photovoltaics at the V. Lashkaryov Institute of Semiconductor Physics. He is the author of more than 70 scientific publications. His main research interests include modeling of silicon solar cells.

<https://orcid.org/0000-0002-7072-6670>; i.o.sokolovskiy@gmail.com



Vlasyuk V.M. PhD, Researcher of the Laboratory of Physical and Technical Fundamentals of Semiconductor Photovoltaics at the V. Lashkaryov Institute of Semiconductor Physics. He is the author of more than 47 scientific publications. The area of his scientific interests includes research,

analysis of silicon solar cells. <https://orcid.org/0000-0001-6352-0423>; viktorvlasiuk@gmail.com



Torchyniuk P.V. Researcher of the Department of Solid State Chemistry, V. Vernadsky Institute of General and Inorganic Chemistry. He is the author of 15 scientific publications. Research interests include the synthesis of organic-inorganic perovskite films $\text{CH}_3\text{NH}_3\text{PbI}_3$ and studying their properties, increasing the stability of

perovskites. <https://orcid.org/0000-0003-2387-3683>;
pasha.torchyniuk@gmail.com



V'yunov O.I. PhD, Senior Scientist, Senior Researcher of the Department of Solid State Chemistry, V. Vernadsky Institute of General and Inorganic Chemistry. He is the author of more than 250 scientific publications. Scientific interests are mostly focused on the synthesis of complex oxide systems and the interrelation between

structural, electrical and physical properties of various functional oxide materials. <https://orcid.org/0000-0001-7420-2287>; vyunov@ionc.kiev.ua



Belous A.G. Doctor of Chemical Sciences, Professor, Head of Department of Solid State Chemistry, V. Vernadsky Institute of General and Inorganic Chemistry, Member of NAS of Ukraine. Authored more than 500 scientific publications. Works in the field of inorganic chemistry and materials science. Investigates the conditions of

formation, structure, properties of complex oxide systems and develops on their basis highly efficient functional materials: ultrahigh-frequency dielectrics, ferroelectric semiconductor materials, cationic conductors for communication systems, mechanical engineering and other branches of industry. <https://orcid.org/0000-0001-7808-3828>;
belous@ionc.kiev.ua



Shkrebtiy A.I. Professor, PhD in Physics and Mathematics, Professor at the University of Ontario, Institute of Technology. The area of his scientific interests includes solid state physics, semiconductors and their surfaces, nanomaterials, nonlinear optical phenomena, electronic, structural and dynamical properties of novel materials.

<https://orcid.org/0000-0002-4998-1538>;
Anatoli.Chkrebtiy@ontariotechu.ca

Вплив співвідношення реагентів на фотоелектричні і оптичні властивості перовскітних плівок для фотовольтаїки

В.П. Костильов, А.В. Саченко, І.О. Соколовський, В.М. Власюк, П.В. Торчинюк, О.І. В'юнов, А.Г. Білоус, А.І. Шкребтій

Анотація. У цій роботі досліджено властивості синтезованих плівок органічно-неорганічних перовскітів $\text{CH}_3\text{NH}_3\text{PbI}_3$, отриманих при різних співвідношеннях вихідних реагентів (PbI_2 and $\text{CH}_3\text{NH}_3\text{I}$). Як розчинник використовували хімічно чистий висушений диметилформамід (ДМФ). Органічно-неорганічні перовскіти є перспективними для застосування в галузі фотовольтаїки. Було показано, що незалежно від співвідношення вихідних реагентів утворюються однофазні перовскіти, при цьому мікроструктура плівок суттєво відрізняється. У роботі досліджено фотоелектричні та оптичні властивості синтезованих плівок, а саме: отримано експериментальні та теоретичні спектральні залежності малосигнальної поверхневої фотонапруги та пропускання. Визначено ширину забороненої зони і залежність параметра Урбаха від співвідношення реагентів. Було встановлено, що ширина забороненої зони отриманих плівок залежить від співвідношення реагентів і дорівнює 1,59, 1,62 та 1,57 еВ, тоді як характерна енергія Урбаха дорівнює 18, 19 та 22 меВ для плівок, отриманих зі співвідношенням $\text{PbI}_2:\text{CH}_3\text{NH}_3\text{I}$ 1:1, 1:2 та 1:3 відповідно. Установлено, що спектральні залежності малосигнальної поверхневої фотонапруги набагато більш чутливі до мікроструктури матеріалу та його електронної структури біля краю поглинання, тоді як оптичні спектри пропускання не такі чутливі. Визначено граничне значення густини струму короткого замикання для плівок, отриманих при різному співвідношенні між PbI_2 та $\text{CH}_3\text{NH}_3\text{I}$.

Ключові слова: перовскіти, спектроскопія поверхневої фотонапруги, оптичні властивості.